Nanoscale

PAPER

View Article Online
View Journal | View Issue

Cite this: *Nanoscale*, 2021, **13**, 9740

Room temperature synthesis of Sn^{2+} doped highly luminescent $CsPbBr_3$ quantum dots for high CRI white light-emitting diodes†

Dongdong Yan,‡ Qionghua Mo,‡ Shuangyi Zhao, Wensi Cai* and Zhigang Zang *

Received 8th March 2021,
Accepted 26th April 2021

DOI: 10.1039/d1nr01492g

rsc.li/nanoscale

With a high photoluminescence quantum yield (PLQY) being able to exceed 90% for those prepared by the hot injection method, $CsPbBr_3$ quantum dots (QDs) have attracted intensive attention for white light-emitting diodes (WLEDs). However, the whole process is carried out in a 3-neck flask *via* air isolation and at a relatively high temperature. In addition, $CsPbBr_3$ QDs suffer from poor stability under ambient atmosphere. In this work, an effective strategy through doping of Sn^{2+} ions at room-temperature is proposed to improve the emission efficiency and stability of $CsPbBr_3$ QDs. Compared with pure $CsPbBr_3$ QDs, a higher PLQY and a better stability are obtained. The detailed physical mechanism for this performance enhancement is discussed and described. An optimum result is found at an Sn^{2+} doping amount of 20%, which shows a high PLQY of 82.77%. WLEDs based on these 20% Sn^{2+} doped $CsPbBr_3$ QDs are also studied, exhibiting a high color rendering index of 89 and a correlated color temperature (CCT) of 3954. The method proposed here provides an effective strategy to enhance the fluorescence and stability of $CsPbBr_3$ QDs, which might have promising potential in the lighting fields.

Introduction

All-inorganic perovskites ($CsPbX_3$, X = Cl, Br, and I) have aroused a great deal of interest in various optoelectronic applications, including solar cells,[1–4] lasers,[5–7] light-emitting diodes (LEDs),[8–14] photodetectors,[15–17] and other areas,[18–20] owing to their outstanding optical properties, namely, tunable and narrow-line width photoluminescence (PL) through the entire visible spectrum,[21] high defect-tolerance,[22] and high photoluminescence quantum yield (PLQY).[23] In the mentioned applications, white-light emitting diodes (WLEDs) based on $CsPbX_3$ quantum dots (QDs) possess unique characteristics of wide colour tunability and good properties of lighting devices. WLEDs typically consist of emitting chips with a coating of green or red perovskite QD materials. Over the past few years, substantial progress has been made in $CsPbX_3$ QD based WLEDs.[24,25] Chen *et al.*[26] employed $CsPbX_3$ QDs to successfully fabricate WLEDs, showing a correlated colour temperature (CCT) of ~5700 and a luminous efficacy of 20 lm W^{-1}. Ren and co-workers[27] prepared WLEDs based on Mn^{2+}-doped $CsPbX_3$ QDs. The fabricated WLEDs showed a CCT of 1918 K and an efficiency of 24 lm W^{-1}. Despite this, $CsPbX_3$-based WLEDs still face the challenge of commercialization.[28] Among $CsPbX_3$ QDs, $CsPbBr_3$ QDs are the most suitable ones in the lighting fields as they possess a higher PL quantum yield (QY) than $CsPbCl_3$ and $CsPbI_3$ QDs. However, the gradual decomposition and prompt quenching under various environmental conditions still limit their practical applications. One effective method to improve the stability of $CsPbBr_3$ QDs is doping. In the past few years, various impurity dopants including Na^+,[29] Cu^{2+},[30] and Ce^{3+} (31) have been reported to enhance the properties of $CsPbBr_3$ QDs. However, the above doping-related methods need heat treatment, inert gas, or pivotal injection operation, and they are not conducive to large-scale fabrication. Hence, it is quite urgent to exploit a room-temperature (RT) synthesis method.

The ionic character of $CsPbBr_3$ QDs allows for doping ions at room temperature. One promising alternative is Sn^{2+}, which has a similar electronic structure and radius to Pb^{2+} cations, making the doping or alloying of Sn in Pb-based perovskite QDs easy.[32] It has been reported that Sn^{2+} doping only narrows the band gap slightly.[33] In addition, Sn^{2+} ions are environmentally friendly and have been reported to replace lead in $CsPbBr_3$ QDs through hot injection (HI) or other complicated methods. Jellicoe[34] and coworkers have successfully synthesized $CsSnBr_3$ QDs using a hot injection method. However, due to the easy oxidation from Sn^{2+} to Sn^{4+} as described by the electron-half-equation $Sn^{2+} \rightarrow Sn^{4+} + 2e^-$, $CsSnBr_3$ perovskite

Key Laboratory of Optoelectronic Technology & Systems (Ministry of Education), Chongqing University, Chongqing 400044, China. E-mail: wensi.cai@cqu.edu.cn, zangzg@cqu.edu.cn

†Electronic supplementary information (ESI) available. See DOI: 10.1039/d1nr01492g

‡These authors contributed equally to this work.

QDs are extremely unstable with a poor optical performance.[35] Also, the hot injection method used above requires a high temperature and an inert atmosphere. The required heating temperature might further cause changes in Sn^{2+} ions. Therefore, it is necessary to develop a facile method to synthesize high quality $CsPbBr_3$ QDs at room temperature using a doping strategy. Although there are some published studies on WLEDs based on $CsPbBr_3$ QDs,[20,21] there is no report on how to achieve high color rendering index (CRI) WLEDs based on B-site doped $CsPbBr_3$ QDs using a facile doping strategy.

Among various doping techniques for $CsPbBr_3$ QDs, the most commonly used ones are hot-injection (HI)[21] and ligand-assisted reprecipitation (LARP).[36] These strategies may improve the stability or optical properties of $CsPbBr_3$ QDs to a certain extent. However, these doping methods still suffer from obvious disadvantages. While the HI method requires high-temperature, and gas protection and might result in high defect formation energy,[37] LARP consumes a large amount of toluene and *N*,*N*-dimethylformide (DMF), which might result in low stability, mixture of morphologies, and broad PL spectra.[38] Herein, we present a facile method to obtain Sn^{2+} doped $CsPbBr_3$ QDs under ambient conditions without adopting most commonly used toluene as an anti-solvent and using a mixed solvent with isopropanol/hexane. To the best of our knowledge, we report here the first demonstration of Sn^{2+} doped $CsPbBr_3$ QDs prepared by a facile method under these solvent conditions. With an optimized doping amount of about 20%, the highest PLQY of 82.77% is obtained. The PL thermostability of this 20% Sn^{2+} doped $CsPbBr_3$ QD film is also enhanced significantly, maintaining 93% of the initial intensity even after being heated at 80 °C for 105 min. WLEDs using the obtained Sn^{2+} doped $CsPbBr_3$ QDs and red AgInZnS QDs as light emitters were also fabricated, exhibiting excellent properties, including a high CRI value of 89 and a CCT of 3954. The facile room temperature methods might also be applicable to other low-toxicity perovskite QDs for enhancing the optical performance and preparing WLEDs at a low cost.

Results and discussion

Fig. 1a shows the $CsPbBr_3$ QD solutions with different doping ratios of Sn^{2+} under both daylight and UV light. The solutions first show an increased brightness with an increase of doping percentage from 0% to 20% and then become turbid and dark upon further increasing the dopant percentage. In order to further analyse the phenomenon, PLQY measurements were performed, as shown in Fig. 1b. While pure $CsPbBr_3$ QD solution exhibits a PLQY value of 54.32%, the doping of Sn^{2+} induces first an increase and then a decrease of the PLQY values. The highest PLQY value of 82.77% is obtained for an Sn^{2+} doping amount of 20%, which is enhanced by 50% compared with the undoped case. Such an improvement might be due to the reduction of defects in Sn^{2+}-doped $CsPbBr_3$ QDs, resulting in a more ordered local environment and the homogeneous distribution of the QDs.[39] Furthermore, the Sn^{2+} ions

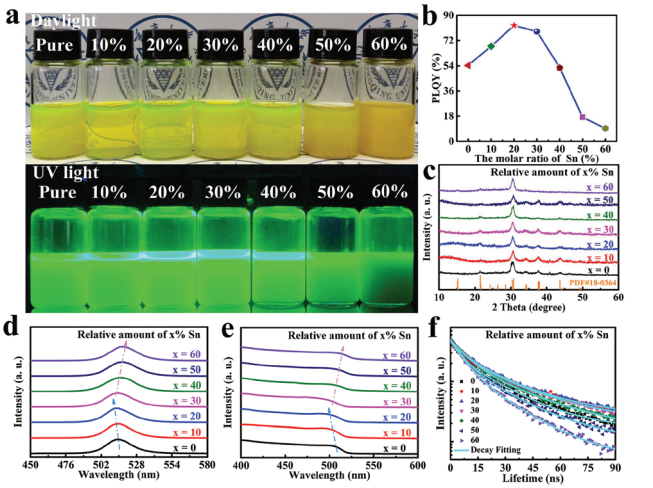

Fig. 1 The comparison of $CsPbBr_3$ QDs with different doping ratios of Sn^{2+}. (a) Solutions under daylight (upper) and UV light (below). (b) PLQY; (c) XRD patterns for different doping ratios of Sn^{2+}. (d) PL spectra, (e) absorption spectra, and (f) time-resolved PL decays of $CsPbBr_3$ QDs.

have been introduced into $CsPbBr_3$ perovskite QDs to replace a part of Pb^{2+} ions, resulting in enhanced PLQY and stability, similar to what were reported previously using other dopant ions.[40,41] Fig. 1c shows the X-ray diffraction (XRD) patterns of the pure and Sn^{2+} doped $CsPbBr_3$ QDs. Three diffraction peaks at 30.7°, 37.9° and 44.1°, corresponding to the (200), (211) and (200) planes, are found in pure $CsPbBr_3$ QDs,[42] indicating a typical cubic structure as suggested by the standard card (JCPDS: 18-0364). With the increase of the Sn^{2+} doping amount from 0 to 50%, no new diffraction peaks appear in the XRD patterns, indicating that the doping has a negligible effect on the structure of QDs. However, when the doping ratio reaches 60%, diffraction peaks at 37.9° and 44.1° disappear, suggesting that the crystallization could be affected if excess Sn^{2+} is used. PL and absorption spectra of the pure and Sn^{2+} doped $CsPbBr_3$ QDs were then recorded to investigate their optical performance. As shown in Fig. 1d, while the PL peak position is at 515 nm with a full width at half maximum (FWHM) of 22 nm (118 meV) for undoped $CsPbBr_3$ QDs, for the doped QDs with x = 10%–60%, the PL peaks are located at 514.3, 512.9, 514.2, 515.9, 516.8, 518.3 nm, respectively. A blue shift in PL spectra is found in the initial stage. This effect is ascribed to the contraction of the original $CsPbBr_3$ QD lattice, resulting in lower absorption abilities and wide band gaps.[43] However, the excess doping and impurity can cause a change of the cubic shape and agglomeration, resulting in a red shift of the spectra on further increasing the Sn doping amount.[44] The corresponding absorption edge values of the samples are 507.9, 503.7, 500.4, 504.6, 507.1, 511.3 and 513.7 nm for x = 0%–60%, respectively, which are in good agreement with the change trend in the PL spectra (see Fig. 1e). The PL decays of pure and Sn^{2+} doped $CsPbBr_3$ QDs as a function of Sn^{2+} doping concentration are shown in Fig. 1f. The PL decay curves are fitted by a bi-exponential decay function, which con-

sists of a fast-decay component (t_1) and a slow-decay component (t_2). A bi-exponential fitting function, $I(t) = A_1 e^{-\frac{t}{t_1}} + A_1 e^{-\frac{t}{t_2}}$ is generally used for the fitting,[10,17] from which, the average lifetime (τ_{ave}) can be obtained using $\tau_{avg} = \frac{A_1 t_1^2 + A_2 t_2^2}{A_1 t_1 + A_2 t_2}$. The corresponding calculated average lifetimes (τ_{avg}) are presented in Table 1, from which an increase of τ_{avg} at an Sn^{2+} doping concentration less than 20% and a decrease of τ_{avg} at an Sn^{2+} doping concentration larger than 20% are clearly seen. The longest average lifetime of 25.26 ns is found in $CsPbBr_3$ QDs doped with 20% Sn^{2+}. In other words, the presence of 20% Sn^{2+} ions increases the radiative recombination channel of $CsPbBr_3$ QDs.

The cubic morphologies of the doped and undoped $CsPbBr_3$ QDs were then studied using transmission electron microscopy (TEM), as shown in Fig. 2 for doping amounts of 0 and 20%. Both samples possess a cubic morphology (see Fig. 2a and b), which is similar to that of previously reported

Table 1 The average lifetimes of Sn^{2+} doped $CsPbBr_3$ QDs

Doping amount of x% Sn	A_1	t_1	A_2	t_2	t_{avg}
0	0.59	4.51	0.41	22.9	18.84
10	0.48	5.11	0.52	27.06	23.8
20	0.52	7.27	0.48	29.98	25.26
30	0.49	7.21	0.51	28.84	24.65
40	0.62	7.17	0.38	27.67	21.58
50	0.62	6.78	0.38	24.99	19.4
60	0.65	6.66	0.35	21.88	16.38

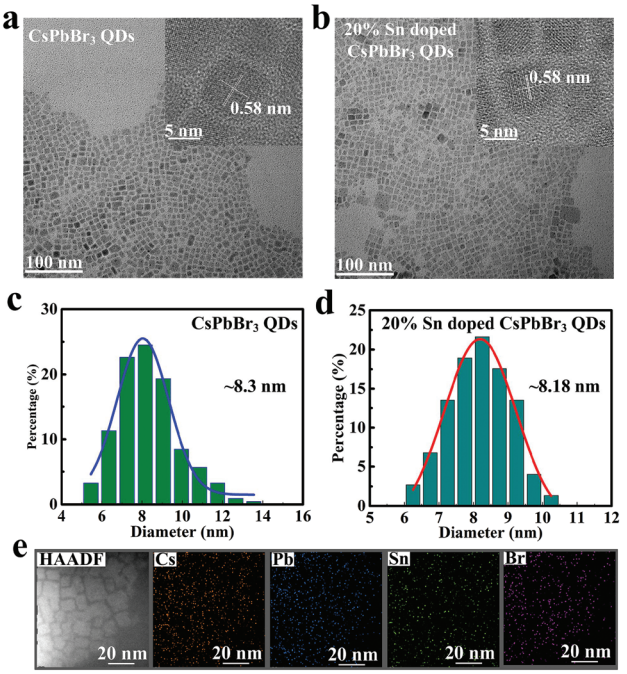

Fig. 2 TEM images of (a) pure $CsPbBr_3$ QDs and (b) 20% Sn^{2+} doping samples, (c) the average size of the pure $CsPbBr_3$ QDs, and (d) 20% Sn^{2+} doping samples. (e) The EDS mapping of 20% Sn doped $CsPbBr_3$ QDs.

$CsPbBr_3$ QDs synthesized from a ligand-assisted reprecipitation method at room temperature.[12] No obvious change in the lattice spacings of the two samples is found, indicating that the amount of Sn^{2+} ion doping here is not enough to change the lattice constant. Fig. 2c and d show the particle size distributions of both samples, from which an average size of 8.3 and 8.18 nm for pure $CsPbBr_3$ QDs and Sn^{2+} doped $CsPbBr_3$ QDs, respectively, are clearly seen. The slightly reduced size here with the doping might be due to the reduced growth rate of the Sn^{2+} doped $CsPbBr_3$ QDs during the reaction, which is similar to the case of perovskite QDs doped with other ions reported previously.[45] In addition, Fig. 2e shows the corresponding EDS mapping of the 20% Sn^{2+} doped $CsPbBr_3$ QDs, demonstrating the presence of Cs, Pb, Br and Sn elements in Sn-doped $CsPbBr_3$ QDs. Fig. S1† shows the corresponding EDS mapping of pure $CsPbBr_3$ QDs. Furthermore, X-ray photoelectron spectra (XPS) of both $CsPbBr_3$ and 20% Sn doped $CsPbBr_3$ QDs were obtained, as shown in Fig. S2.† The XPS results of 20% Sn doped $CsPbBr_3$ clearly demonstrate peaks at ~490 eV, which correspond to Sn 3d and suggest the presence of Sn^{2+} in the lattice.

Stability is one of the most important characteristics in realizing commercialization, and to study it, PL stabilities of pure $CsPbBr_3$ QDs and 20% Sn^{2+} doped $CsPbBr_3$ QD samples were studied at a temperature of 80 °C in air, as shown in Fig. 3. The PL intensity of the pure $CsPbBr_3$ QD film drops to 14% of the initial value when heated at 80 °C for 105 min (Fig. 3a). In contrast, the PL intensity of the doped sample shows a slow decrease under the same test conditions, maintaining about 93% of the initial value after 105 min (Fig. 3b), with nearly no redshift being found in the peak position. Such an enhanced thermostability of Sn^{2+} doped QDs might be due to the effective passivation of surface defect states through the Sn^{2+} ion doping into $CsPbBr_3$ QDs.

According to our previous reports, $CsPbBr_3$ QDs with improved stability are conducive to optical device fabrication, including WGM lasers and LEDs.[46–48] The high PLQYs and the excellent thermal stability make doped $CsPbBr_3$ QDs attractive candidates as pure green constituents in white LEDs (WLEDs). To demonstrate this, WLEDs using green $CsPbBr_3$ QDs (doped and undoped), red emissive phosphor AgInZnS QDs, and blue InGaN chips were fabricated. The same amount of green QDs

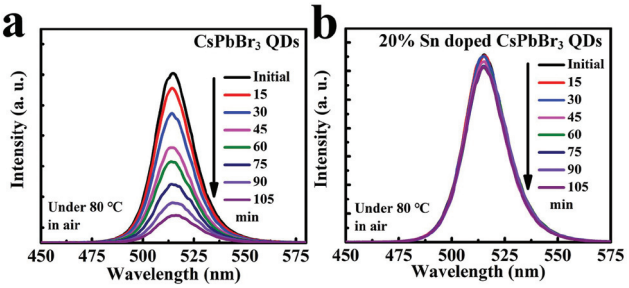

Fig. 3 PL stability of (a) pure $CsPbBr_3$ QDs and (b) 20% Sn^{2+} doped $CsPbBr_3$ QDs at 80 °C.

with the same concentration of 15 mg ml^{-1} was used in the fabrication process to ensure nearly the same thickness. The spectra of WLEDs based on pure $CsPbBr_3$ QDs and Sn^{2+} doped $CsPbBr_3$ QDs are shown in Fig. 4a and b. The ratio of the green ingredient in 20% Sn^{2+} doped $CsPbBr_3$ QD-WLEDs is obviously higher than that of pure $CsPbBr_3$ QD-WLEDs, owing to the high PLQY in 20% Sn^{2+} doped $CsPbBr_3$ QDs. Both devices show peaks at 450, 520 and 610 nm, corresponding to blue InGaN chip, $CsPbBr_3$ QDs and AgInZnS QDs, respectively. WLEDs based on pure $CsPbBr_3$ QDs show a luminous efficiency of 32.8 lm W^{-1} with an international de L'Eclarage (CIE) colour coordinate value of (0.38, 0.34) at a driving voltage of 2.5 V, as shown in Fig. 4b. In contrast, WLEDs based on Sn^{2+} doped $CsPbBr_3$ QDs show a higher luminous efficiency of 43.2 lm W^{-1} with a CIE colour coordinate value of (0.41, 0.48) (see Fig. 4c). The CRI of WLEDs based on Sn^{2+} doped $CsPbBr_3$ QDs is also found to be much higher than those based on pure $CsPbBr_3$ QDs. The detailed parameters of the fabricated WLEDs are presented in Table 2. The performance of the fabricated WLEDs was then compared with those of other $CsPbBr_3$ QD-based WLEDs, as shown in Table 3. It is found that the CRI value of our optimized WLEDs here is the highest value compared to those in other reported publications.

The properties of WLEDs with an increase of driving voltages were also studied, as shown in Fig. S3 and S4.† While pure $CsPbBr_3$ QD based WLEDs show a decrease of the green-to-blue intensity ratio from 0.95 to 0.67 with the increase of driving voltage from 2.5 to 2.8 V, for those with Sn^{2+} doped $CsPbBr_3$ QDs it increases from 6.6 to 9.4 (Fig. S4†). Also, the blue light excited by InGaN chips is absorbed by the Sn^{2+} doped $CsPbBr_3$ QDs. WLEDs based on pure $CsPbBr_3$ QDs show CIE colour coordinates of (0.38, 0.34) at a driving voltage of 2.5 V and (0.37, 0.31) at 2.8 V, suggesting a low stability. In contrast, WLEDs based on Sn^{2+} doped $CsPbBr_3$ QDs exhibit more stable CIE behaviours with the increase of driving voltages, suggesting less degradation of $CsPbBr_3$ QDs under strong illumination. The results therefore clearly suggest that Sn^{2+} doped $CsPbBr_3$ QDs have advantages over regular $CsPbBr_3$ QDs for applications in WLEDs.

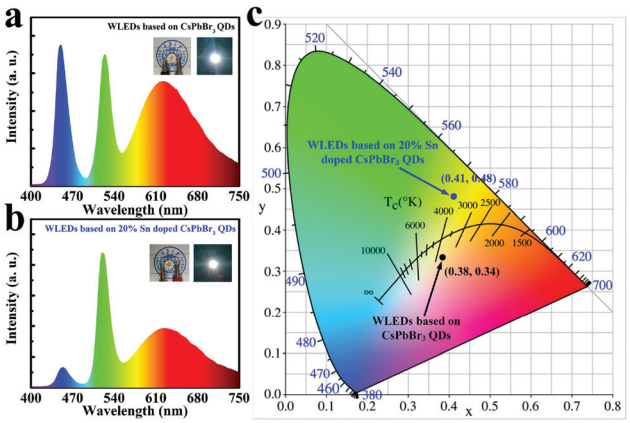

Fig. 4 PL spectra of WLEDs based on (a) $CsPbBr_3$ QDs and (b) 20% Sn^{2+} doped $CsPbBr_3$QDs. (c) CIE chromaticity diagram of both WLEDs.

Table 2 Optical parameters of WLEDs based on $CsPbBr_3$ QDs

Groups	CRI	CCT (K)	Efficiency (lm W^{-1})	CIE coordinates (X, Y)
$CsPbBr_3$	80	3556	32.8	(0.38, 0.34)
20% Sn doping $CsPbBr_3$	89	3954	43.2	(0.41, 0.48)

Conclusions

In summary, we report a facile room temperature method to synthesize Sn^{2+} doped $CsPbBr_3$ QDs without using most commonly used toluene as an anti-solvent. The optimized QDs showed a high PLQY of 82.77% and a significantly enhanced thermal stability. Such modified QDs were also studied in WLEDs by combining with red AgInZnS QDs on InGaN blue chips, and they showed excellent luminescence performance, including colour coordinates of (0.41, 0.48), a high colour rendering index of 89 and a power efficiency of 43.2 lm W^{-1}. These Sn $^{2+}$ doped $CsPbBr_3$ QDs and the preparation method might have great potential in the optical fields where low cost and high performance are required.

Experimental section

Chemicals and reagents

Lead bromide ($PbBr_2$, 99.99%), cesium carbonate (Cs_2CO_3, 99.9%), tin(II) bromide ($SnBr_2$, 99.2%), oleylamine (OAm, 90%), *N*,*N*-dimethylformamide (DMF), 2-propanol (IPrOH, 99.5%), propionic acid (PrAc, 99.5%), hexane (HEX, 95%), and OAm (>90%, Aladdin) were used. silver nitrate ($AgNO_3$, 99.8%, Aldrich), zinc stearate ($Zn(St)_2$, 90%, Aldrich), *n*-dodecylthiol

Table 3 Comparison of the main optical parameters in WLEDs based on $CsPbBr_3$ QDs

Color-converting materials	Method	Power efficiency (lm W^{-1})	CRI	CCT	Refs.
$CsPbBr_3$@glass + $CsPbBr_2I$@glass	Melting (700 °C)	20	84	5700	26
$CsPbBr_3$ + $BaGe_4O_9:Eu^{3+}$ phosphors	HI	38.89	—	4033	49
$CsPbBr_3$ + $CsPb(Br/I)_3$	HI	14.1	81	—	50
$CsPbBr_3$ + $Cs_2GeF_6:Mn^{4+}$	HI	27.3	81.4	—	51
Al:$CsPbBr_3$ + CdSe@ZnS	HI	21.6	—	—	52
Sn^{2+} doped $CsPbBr_3$ + AgInZnS	RT	43.2	89	3954	This work

(DDT, 99.8%, Aladdin), sulfur (S, 99.9%, Aldrich), and indium acetate ($In(Ac)_3$, 99.9%, Aldrich) were used without further purification.

Synthesis of $CsPbBr_3$ QDs and Sn doped $CsPbBr_3$ QDs

The Sn^{2+} ion doping strategy has been developed based on a modification of the synthesis method reported by Akkerman.[53] First, 3 mL of hexane was added into 3 mL of 2-propanol to form a mixed solution (solution 1). Cs-PrAc precursor solution was prepared by dissolving 0.9 mmol of Cs_2CO_3 in 0.5 ml of PrAc followed by stirring for 30 min to obtain a clear solution of the mixture (solution 2). $PbBr_2$ precursor solution was prepared by dissolving 0.105 mmol of $PbBr_2$ in 1 ml of 1 : 1 : 1 IPrOH : PrAc : DMF (solution 3). To prepare $CsPbBr_3$ QDs, solution 2 was added into solution 1, followed by an injection of solution 3 into the mixture to react for 5–10 s. The preparation was done entirely at room temperature. The synthesis of Sn^{2+} doped $CsPbBr_3$ QDs was similar to that of $CsPbBr_3$ QDs, except that $SnBr_2$ and $PbBr_2$ with a specific molar ratio were mixed in the above solution 3.

Synthesis of AgInZnS QDs

0.4 mmol of $In(Ac)_3$ and 0.1 mmol of $AgNO_3$ were added into a mixture solution of ODE (4 mL), OA (0.2 mL) and dodecanethiol (0.75 mL) in a 50 mL three-neck flask 1 and heated to 60 °C under a nitrogen gas flow. Meanwhile, 0.5 mmol of sulfur was dissolved in a mixture solution of OAm (0.5 mL) and ODE (0.5 mL) in bottle 1. $Zn(St)_2$ (0.5 mmol) was dissolved in a mixture solution containing OAm (0.5 mL) and ODE (0.5 mL) in bottle 2. After 30 min, the mixture solution in flask 1 was heated to 90 °C for 10 min, followed by a quick injection with the solution in bottle 1. Flask 1 temperature was then raised to 115 °C, with the $Zn(St)_2$ precursors in bottle 2 slowly added dropwise. The reaction solution was kept at 115 °C for 35 min to allow the growth of AgInZnS QDs. Upon completion, the crude solution was cooled to room temperature. For purification, the crude reaction solution was centrifuged at 9500 rpm for 10 min after adding some toluene. The obtained supernatant was added into ethanol solvents with a volume ratio of 1 : 3 and precipitated again, and the supernatant was discarded to obtain the purified AgInZnS QDs.

Characterization of materials

The crystallinity was tested by powder XRD (XRD-6100, Shimadzu, Japan) with monochromatized Cu Kα radiation. TEM images were obtained using an electron microscope (Libra 200 FE, Zeiss, Germany). Absorption spectral measurements were performed by using a UV–vis spectrophotometer (UV–vis: UV-2100, Shimadzu, Japan). PL spectroscopy was performed using a fluorescence spectrophotometer (PL: Agilent Cary Eclipse, Australia). FTIR analysis (KBr pellet method) was performed with a Nicolet iS50 FT-IR spectrometer (Thermo Fisher Scientific, Waltham, MA, USA) to characterize the product structure of EJTLE. TRPL decay curves were obtained using an Edinburgh FLS1000 system. XPS analysis was performed using an Escalab 250 Xi system. The performances of the fabricated WLEDs were measured using a spectrograph of PR670 with an analyzer system.

Fabrication of white LED devices

10 mg of polymethyl methacrylate (PMMA) and 20 mg of $CsPbBr_3$ QDs were dissolved together in 20 mL of toluene and stirred for 24 h. Similarly, both PMMA (10 mg) and AgInZnS QDs (25 mg) were dissolved in 20 mL of toluene and stirred for 24 h. The WLEDs were fabricated by using the above two solutions on the InGaN chip.

Conflicts of interest

The authors declare no conflict of interest.

Acknowledgements

This work was financially supported by the National Natural Science Foundation of China (11974063 and 61904023), Key Program Science Foundation of Natural Science Foundation of Chongqing (cstc2020jcyj-jqX0028), Postdoctoral Science Foundation of China (2019M653336, 2020M683242) and Chongqing Special Postdoctoral Science Foundation (cstc2019jcyj-bshX0078 and cstc2020jcyj-bshX0123). We thank the Analytical and Testing Centre of Chongqing University for some measurements.

Notes and references

1 F. Liu, C. Ding, Y. Zhang, T. S. Ripolles, T. Kamisaka, T. Toyoda, S. Hayase, T. Minemoto, K. Yoshino, S. Dai, M. Yanagida, H. Noguchi and Q. Shen, *J. Am. Chem. Soc.*, 2017, **139**, 16708–16719.
2 A. Swarnkar, A. R. Marshall, E. M. Sanehira, B. D. Chernomordik, D. T. Moore, J. A. Christians, T. Chakrabarti and J. M. Luther, *Science*, 2016, **354**, 92–95.
3 H. Wang, H. Li, S. Cao, M. Wang, J. Chen and Z. Zang, *Sol. RRL*, 2020, **4**, 2000226.
4 X. Hu, H. Wang, Y. Ying, M. Wang, C. Zhang, Y. Ding, H. Li, W. Li, S. Zhao and Z. Zang, *J. Power Sources*, 2020, **480**, 229073.
5 H. Zhu, Y. Fu, F. Meng, X. Wu, Z. Gong, Q. Ding, M. V. Gustafsson, M. T. Trinh, S. Jin and X. Y. Zhu, *Nat. Mater.*, 2015, **14**, 636–642.
6 G. Xing, N. Mathews, S. S. Lim, N. Yantara, X. Liu, D. Sabba, M. Grätzel, S. Mhaisalkar and T. C. Sum, *Nat. Mater.*, 2014, **13**, 476–480.
7 Y. Wang, X. Li, J. Song, L. Xiao, H. Zeng and H. Sun, *Adv. Mater.*, 2015, **27**, 7101–7108.
8 X. Zhang, H. Lin, H. Huang, C. Reckmeier, Y. Zhang, W. C. H. Choy and A. L. Rogach, *Nano Lett.*, 2016, **16**, 1415–1420.

9 M. Lu, X. Zhang, X. Bai, H. Wu, X. Shen, Y. Zhang, W. Zhang, W. Zheng, H. Song, W. W. Yu and A. L. Rogach, *ACS Energy Lett.*, 2018, **3**, 1571–1577.
10 J. Li, L. Xu, T. Wang, J. Song, J. Chen, J. Xue, Y. Dong, B. Cai, Q. Shan, B. Han and H. Zeng, *Adv. Mater.*, 2017, **29**, 1603885.
11 J. Si, Y. Liu, Z. He, H. Du, K. Du, D. Chen, J. Li, M. Xu, H. Tian, H. He, D. Di, C. Lin, Y. Cheng, J. Wang and Y. Jin, *ACS Nano*, 2017, **11**, 11100–11107.
12 J. Pan, L. N. Quan, Y. Zhao, W. Peng, B. Murali, S. P. Sarmah, M. Yuan, L. Sinatra, N. M. Alyami, J. Liu, E. Yassitepe, Z. Yang, O. Voznyy, R. Comin, M. N. Hedhili, O. F. Mohammed, Z. H. Lu, D. H. Kim, E. H. Sargent and O. M. Bakr, *Adv. Mater.*, 2016, **28**, 8718–8725.
13 G. Li, F. W. R. Rivarola, N. J. L. K. Davis, S. Bai, T. C. Jellicoe, F. de la Peña, S. Hou, C. Ducati, F. Gao, R. H. Friend, N. C. Greenham and Z.-K. Tan, *Adv. Mater.*, 2016, **28**, 3528–3534.
14 J. Song, J. Li, X. Li, L. Xu, Y. Dong and H. Zeng, *Adv. Mater.*, 2015, **27**, 7162–7167.
15 X. Li, D. Yu, F. Cao, Y. Gu, Y. Wei, Y. Wu, J. Song and H. Zeng, *Adv. Funct. Mater.*, 2016, **26**, 5903–5912.
16 Y. Dong, Y. Gu, Y. Zou, J. Song, L. Xu, J. Li, J. Xue, X. Li and H. Zeng, *Small*, 2016, **12**, 5622–5632.
17 C. Han, C. Li, Z. Zang, M. Wang, K. Sun, X. Tang and J. Du, *Photonics Res.*, 2017, **5**, 473–480.
18 V. Caligiuri, M. Palei, M. Imran, L. Manna and R. Krahne, *ACS Photonics*, 2018, **5**, 2287–2294.
19 S. Yakunin, D. N. Dirin, Y. Shynkarenko, V. Morad, I. Cherniukh, O. Nazarenko, D. Kreil, T. Nauser and M. V. Kovalenko, *Nat. Photonics*, 2016, **10**, 585–589.
20 Z. Nie, X. Gao, Y. Ren, S. Xia, Y. Wang, Y. Shi, J. Zhao and Y. Wang, *Nano Lett.*, 2020, **20**, 4610–4617.
21 L. Protesescu, S. Yakunin, M. I. Bodnarchuk, F. Krieg, R. Caputo, C. H. Hendon, R. X. Yang, A. Walsh and M. V. Kovalenko, *Nano Lett.*, 2015, **15**, 3692–3696.
22 M. V. Kovalenko, L. Protesescu and M. I. Bodnarchuk, *Science*, 2017, **358**, 745–750.
23 Q. A. Akkerman, V. D'Innocenzo, S. Accornero, A. Scarpellini, A. Petrozza, M. Prato and L. Manna, *J. Am. Chem. Soc.*, 2015, **137**, 10276–10281.
24 S. A. Veldhuis, P. P. Boix, N. Yantara, M. Li, T. C. Sum, N. Mathews and S. G. Mhaisalkar, *Adv. Mater.*, 2016, **28**, 6804–6834.
25 H. Guan, S. Zhao, H. Wang, D. Yan, M. Wang and Z. Zang, *Nano Energy*, 2020, **67**, 104279.
26 D. Chen, S. Yuan, X. Chen, J. Li, Q. Mao, X. Li and J. Zhong, *J. Mater. Chem. C*, 2018, **6**, 6832–6839.
27 J. Ren, X. Zhou and Y. Wang, *Nano Res.*, 2020, **13**, 3387–3395.
28 Z. Shi, Y. Li, S. Li, X. Li, D. Wu, T. Xu, Y. Tian, Y. Chen, Y. Zhang, B. Zhang, C. Shan and G. Du, *Adv. Funct. Mater.*, 2018, **28**, 1870135.
29 S. Li, Z. Shi, F. Zhang, L. Wang, Z. Ma, D. Yang, Z. Yao, D. Wu, T.-T. Xu, Y. Tian, Y. Zhang, C. Shan and X. J. Li, *Chem. Mater.*, 2019, **31**, 3917–3928.
30 C. Bi, S. Wang, Q. Li, S. V. Kershaw, J. Tian and A. L. Rogach, *J. Phys. Chem. Lett.*, 2019, **10**, 943–952.
31 J.-S. Yao, J. Ge, B.-N. Han, K.-H. Wang, H.-B. Yao, H.-L. Yu, J.-H. Li, B.-S. Zhu, J.-Z. Song, C. Chen, Q. Zhang, H.-B. Zeng, Y. Luo and S.-H. Yu, *J. Am. Chem. Soc.*, 2018, **140**, 3626–3634.
32 B. Zhao, M. Abdi-Jalebi, M. Tabachnyk, H. Glass, V. S. Kamboj, W. Nie, A. J. Pearson, Y. Puttisong, K. C. Gödel, H. E. Beere, D. A. Ritchie, A. D. Mohite, S. E. Dutton, R. H. Friend and A. Sadhanala, *Adv. Mater.*, 2017, **29**, 1604744.
33 J. Yu, J. Kong, W. Hao, X. Guo, H. He, W. R. Leow, Z. Liu, P. Cai, G. Qian, S. Li, X. Chen and X. Chen, *Adv. Mater.*, 2019, **31**, 1806385.
34 T. C. Jellicoe, J. M. Richter, H. F. J. Glass, M. Tabachnyk, R. Brady, S. E. Dutton, A. Rao, R. H. Friend, D. Credgington, N. C. Greenham and M. L. Böhm, *J. Am. Chem. Soc.*, 2016, **138**, 2941–2944.
35 M. M. Tavakoli, S. M. Zakeeruddin, M. Grätzel and Z. Fan, *Adv. Mater.*, 2018, **30**, 1705998.
36 X. Li, Y. Wu, S. Zhang, B. Cai, Y. Gu, J. Song and H. Zeng, *Adv. Funct. Mater.*, 2016, **26**, 2435–2445.
37 D. Yang and D. Huo, *J. Mater. Chem. C*, 2020, **8**, 6640–6653.
38 H. Huang, Y. Li, Y. Tong, E.-P. Yao, M. W. Feil, A. F. Richter, M. Döblinger, A. L. Rogach, J. Feldmann and L. Polavarapu, *Angew. Chem., Int. Ed.*, 2019, **58**, 16558–16562.
39 Z.-J. Yong, S.-Q. Guo, J.-P. Ma, J.-Y. Zhang, Z.-Y. Li, Y.-M. Chen, B.-B. Zhang, Y. Zhou, J. Shu, J.-L. Gu, L.-R. Zheng, O. M. Bakr and H.-T. Sun, *J. Am. Chem. Soc.*, 2018, **140**, 9942–9951.
40 W. van der Stam, J. J. Geuchies, T. Altantzis, K. H. W. van den Bos, J. D. Meeldijk, S. Van Aert, S. Bals, D. Vanmaekelbergh and C. de Mello Donega, *J. Am. Chem. Soc.*, 2017, **139**, 4087–4097.
41 S. Das, A. De and A. Samanta, *J. Phys. Chem. Lett.*, 2020, **11**, 1178–1188.
42 X. Yu, Y. Wang, J. Zhang, J. Duan, X. Yang, L. Liu and Q. Tang, *J. Mater. Chem. A*, 2020, **8**, 14299–14307.
43 W. van der Stam, J. J. Geuchies, T. Altantzis, K. H. W. van den Bos, J. D. Meeldijk, S. Van Aert, S. Bals, D. Vanmaekelbergh and C. de Mello Donega, *J. Am. Chem. Soc.*, 2017, **139**, 4087–4097.
44 S. Bera, D. Ghosh, A. Dutta, S. Bhattacharyya, S. Chakraborty and N. Pradhan, *ACS Energy Lett.*, 2019, **4**, 1364–1369.
45 Y. Hu, X. Zhang, C. Yang, J. Li and L. Wang, *RSC Adv.*, 2019, **9**, 33017–33022.
46 D. Yan, T. Shi, Z. Zang, T. Zhou, Z. Liu, Z. Zhang, J. Du, Y. Leng and X. Tang, *Small*, 2019, **15**, 1901173.
47 D. Yan, T. Shi, Z. Zang, S. Zhao, J. Du and Y. Leng, *Chem. Eng. J.*, 2020, **401**, 126066.
48 D. Yan, S. Zhao, H. Wang and Z. Zang, *Photonics Res.*, 2020, **8**, 1086–1092.
49 H. Ding, W. Liu, Y. Zheng, C. Li, H. Jiang and X. Wang, *J. Mater. Chem. C*, 2019, **7**, 1690–1695.

50 H. Huang, B. Chen, Z. Wang, T. F. Hung, A. S. Susha, H. Zhong and A. L. Rogach, *Chem. Sci.*, 2016, **7**, 5699–5703.
51 Y. Wei, K. Li, Z. Cheng, M. Liu, H. Xiao, P. Dang, S. Liang, Z. Wu, H. Lian and J. Lin, *Adv. Mater.*, 2019, **31**, 1807592.
52 M. Liu, G. Zhong, Y. Yin, J. Miao, K. Li, C. Wang, X. Xu, C. Shen and H. Meng, *Adv. Sci.*, 2017, **4**, 1700335.
53 Q. A. Akkerman, M. Gandini, F. Di Stasio, P. Rastogi, F. Palazon, G. Bertoni, J. M. Ball, M. Prato, A. Petrozza and L. Manna, *Nat. Energy*, 2016, **2**, 16194.